How to cite: *Angew. Chem. Int. Ed.* **2023,** *62,* e202300658
International Edition: doi.org/10.1002/anie.202300658
German Edition: doi.org/10.1002/ange.202300658

Supramolecular Networks

Spontaneous Chirality Induction in the Assembly of a Single Layer 2D Network with Switchable Pores

Bowen Shen, Chunyu Pan, Xiaopeng Feng, Jehan Kim, Mo Sun, and Myongsoo Lee**

Abstract: Although two-dimensional (2D) chiral sheet structures are attractive because of their unique chemical and physical properties, single layer 2D chiral network structures with switchable pore interior remain elusive. Here we report spontaneous chirality induction in a single layer 2D network structure formed from the self-assembly of tetrapod azobenzene molecules. The chirality induction arises from multiple sublayers slipped in a preferred direction in which the sublayer consists of unidentical molecular arrangements in the in-plane a and b directions, breaking both the plane of symmetry and inversion symmetry. The protruded azobenzene units in the pore interior can be selectively isomerized upon UV irradiation, resulting in a reversible deformation of the chiral pores while maintaining the 2D frameworks. The chiral network can thus selectively entrap one enantiomer from a racemic solution with near perfect enantioselectivity, and then release it upon UV irradiation.

Introduction

The desire to create porous network materials with precise control over the organization of molecular building blocks has stimulated great effort over the past decade in the fields of chemistry, materials science, and nanotechnology.[1–3] This has led to the emergence of reticular chemistry dealing with the design of chemically programmed network structures including metal–organic frameworks (MOFs),[4] covalent-organic frameworks (COFs),[5] hydrogen-bonded organic frameworks (HOFs),[6] and supramolecular organic frameworks (SOFs).[7–9] Among the various network structures, two-dimensional (2D) structures with chiral arrangements are attracting particular attention due to their unique properties originating from their optically active pore interior together with a large surface area. The 2D network structures can be produced by the exfoliation of multi-layered MOF/COF structures,[10,11] the self-assembly of multi-pod aromatic building blocks,[12,13] and surface-assisted synthesis.[14,15] Nevertheless, most of the 2D layers do not exhibit properties related to optical activities, since such framework design encounters difficulties in breaking mirror symmetry in two dimensions.[16] To date, only a few approaches to induce chirality in 2D layered materials have been reported.[17,18] For example, the twist stacks of single-layered objects can be an approach for mirror symmetry breaking, as exemplified in a twist stacking of bilayer graphene.[19,20] This principle for symmetry breaking can be extended to dimeric macrocycle stacks generating chiral pores. For example, twisted macrocycle dimers can induce pore chirality by breaking mirror symmetry.[21,22] The subsequent lateral assembly of the dimeric macrocycle forms single-layered chiral sheet structures. Another approach to single-layered chiral sheets is provided by the lateral association of helical one-dimensional (1D) objects, which provide chiral void spaces. For example, fibrous α-helical peptides can be aligned parallel to each other to form 2D chiral sheet structures.[23] Considering the parallel arrangements of the helical fibers, the void spaces formed between the 2D fiber arrangements are chiral, which discriminate one enantiomer from racemic mixture solution. Recently, we reported the formation of chiral 2D sheet structures with dual chiral void spaces by self-assembly of rectangular-shaped coplanar aromatic amphiphiles.[24] The chirality of the sheets is induced by a slipped-cofacial stack of rectangular-shaped coplanar aromatic segments with a preferred direction in clusters that are arranged laterally with up and down in-plane packing, resulting in dual chiral void spaces. Notably, the single-layered chiral nanosheets can function as highly efficient enantiomer absorbing nanomaterials which absorb exclusively one enantiomer in a racemic mixture solution. Despite such notable examples of chiral 2D materials, spontaneous chirality induction in single-layered networks with switchable pores remains elusive. Here, we report single layer chiral 2D network structures with photo-switchable internal cavities formed by self-assembly of azobenzene-based tetrapod aromatic amphiphiles in aqueous methanol solution. The single layer 2D network consists of quadruple sublayers slipped with a preferred direction in which the sublayer has different molecular arrangements in in-plane a and b directions, breaking both plane of symmetry and inversion symmetry,

[*] Dr. B. Shen, Dr. M. Sun, Prof. M. Lee
Department of Chemistry, Shanghai Key Laboratory of Molecular Catalysis and Innovative Materials, Fudan University
Shanghai 200438 (China)
E-mail: mosun@fudan.edu.cn
mslee@fudan.edu.cn

C. Pan, X. Feng
State Key Laboratory of Supramolecular Structure and Materials, College of Chemistry, Jilin University
Changchun 130012 (China)

J. Kim
Pohang Accelerator Laboratory, POSTECH
Pohang, Gyeongbuk (Korea)

resulting in chirality induction in 2D network structure. The self-assembly of tetrapod aromatic segments endows 2D network structure with protruded azobenzene units in the pore interiors. Thus, light irradiation triggers selective photoisomerization of the azobenzene units of the protruded parts, resulting in the reversible deformation of the chiral pores while maintaining 2D network frameworks (Figure 1). The switchable chiral networks are able to selectively entrap one enantiomer from a racemic solution with near perfect enantioselectivity and then release upon UV irradiation.

Results and Discussion

The molecules that form single layer chiral networks consist of a tetrapod aromatic segment bearing azobenzene units and oligoether dendrons grafted at both sides of the aromatic plane were synthesized in a stepwise manner according to the procedures described in Supporting Information. The resulting amphiphilic molecules were characterized by ^{1}H- and ^{13}C NMR spectroscopies, and MALDI-TOF mass spectroscopy which were shown to be in full agreement with the chemical structure presented (Figures S1,S2). The formation of self-assembled nanostructures of the aromatic amphiphile was investigated with the aqueous methanol solution (3/7, v/v) of **1** using transmission electron microscopy (TEM) and atomic force microscopy (AFM). When subjected to cryogenic TEM (cryo-TEM) using a frozen solution, the image showed flat 2D sheet objects with straight edges (Figure 2a), indicating that **1** self-assembles into a 2D flat sheet structure in bulk solution. To obtain additional structural information on the sheets, TEM experiments were performed with negatively stained films (Fig-

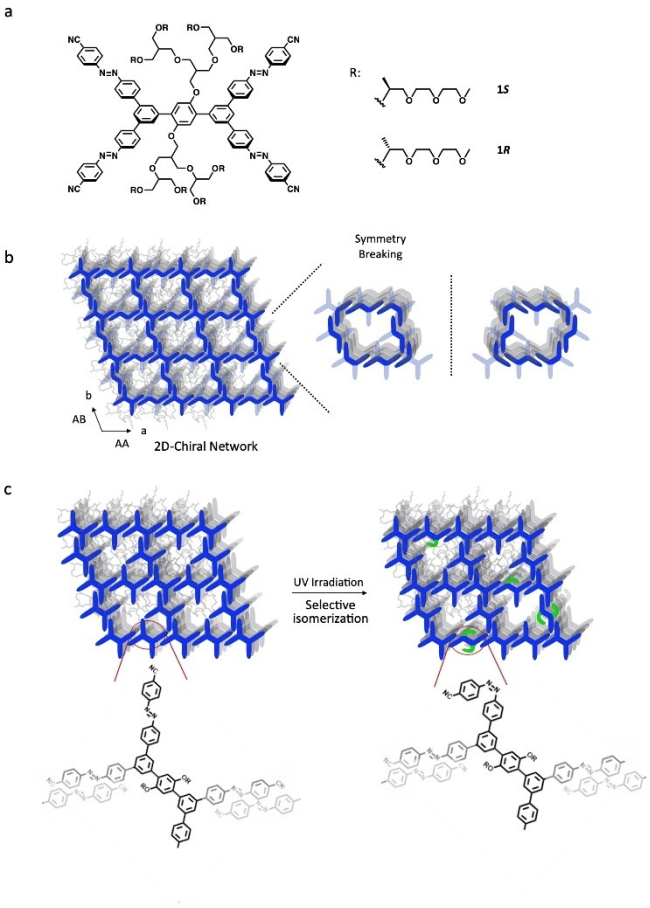

Figure 1. a) Molecular structure of **1**. b) Schematic representation of the formation of a 2D chiral network structure through hierarchical assembly of clusters consisting of slipped planar aromatic segments. c) Switchable cavities with selective isomerization upon UV irradiation.

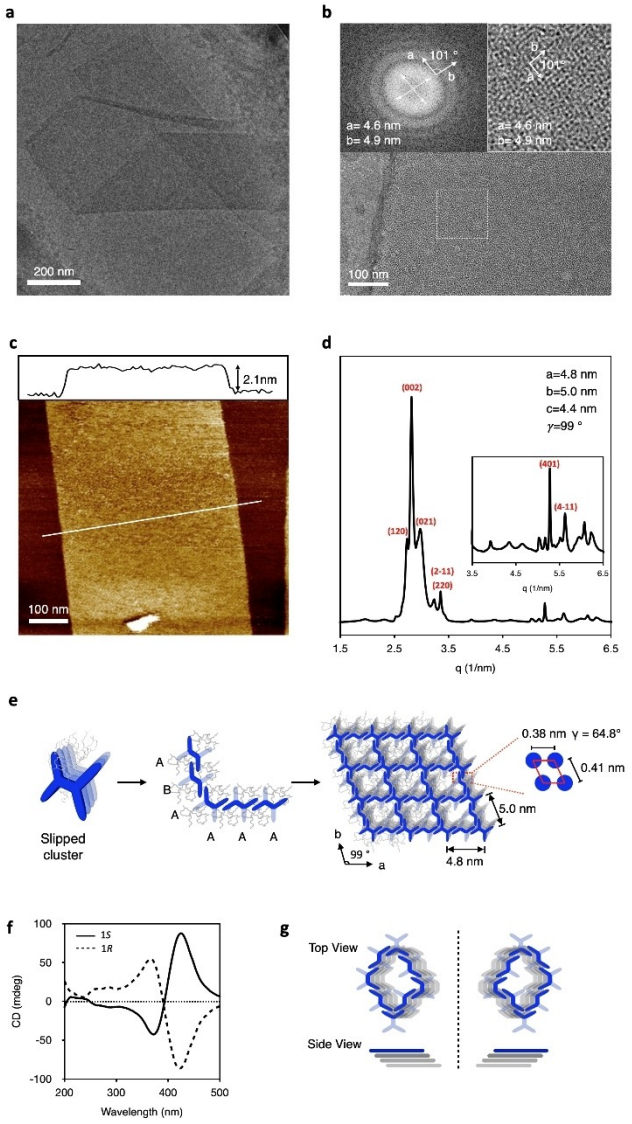

Figure 2. a) Cryo-TEM image of **1*S*** (0.01 wt%) in aqueous methanol solution (3/7, v/v). b) Negatively stained TEM image from the cast film of **1*S***; inset: left: 2D Fourier transformation of ordered pores; right: high-resolution TEM image of **1*S***. c) AFM height image of the sheets on a mica surface from evaporation of **1*S*** (0.01 wt%) in aqueous methanol solution (3/7, v/v). The cross-sectional profile (top) is taken along the white line. d) SAXS pattern of **1*S*** with a freeze-dried sample. e) Schematic illustration of the sheet formed from lateral assembly of slipped clusters. f) CD spectra of **1*S*** (solid) and **1*R*** (dash) (0.01 wt%) aqueous methanol solution (3/7, v/v). g) Schematic illustration of the mirror relationship of the chiral pore packing model.

ure 2b). The image revealed flat 2D sheet structures with straight edges, consistent with the cryo-TEM result. A high-resolution TEM image revealed 2D organized network structures with an oblique lattice with in-plane dimensions of $a=4.6$ nm and $b=4.9$ nm. AFM investigations showed that the networks are very flat with a uniform thickness of 2.1 nm (Figure 2c). To gain further insight into the 2D network structure, X-ray experiments were performed with freeze-dried samples of **1** (Figure 2d), which maintains the self-assembled structure during the drying process. Small-angle X-ray scatterings (SAXS) showed a number of sharp reflections which agree well with the expected relative peak positions for a 3D base-centered monoclinic structure with lattice parameters of $a=4.8$ nm, $b=5.0$ nm, $c=4.4$ nm, and $\gamma=99°$ (Table S1), which was further confirmed by grazing-incidence SAXS (GI-SAXS) (Figure S3). Equidistant diffractions in GI-SAXS were observed at both the equator and meridian. The signals from equatorial diffractions correspond to in-plane order, which is well-matched with the images determined from TEM experiments. Considering the layer thickness of 2.1 nm obtained from AFM investigation, the meridian diffraction corresponding to layer stacks of 4.4 nm indicates that the single layered networks with a 2D oblique lattice are stacked in an ABAB manner. The wide-angle X-ray diffraction pattern shows sharp reflections associated with π–π stacks with lattice dimensions of $a=0.41$ nm, $b=0.37$ nm, and $\gamma=64.8°$, indicative of the crystal packing of the slipped aromatic segments in the network structure (Figure S4).

Taking into account the lattice parameters and the measured density of 1.12 g ml^{-1}, the number of molecules consisting of a pore can be estimated to be 12 (Table S2). Considering the molecular size of **1** and the network thickness, this suggests that the primary structure consists of four molecules in which the aromatic segments stack on top of one another with slipping in a preferred direction (Figure 3a). Subsequently, the aromatic clusters with aromatic side face self-assemble laterally with AA packing in *a*-axis and AB packing in *b*-axis to form a network structure with protruded azobenzene units (Figure 2e). Thus, the network layer consists of quadruple sublayer stacks which slip over each other. This 2D arrangement of a flat tetrapod aromatic segments into slipped sublayers with unidentical packings in in-plane a and b axes leads to symmetry breaking to induce chirality in the 2D network structure.[25] It is noteworthy that the protruded azobenzene parts directly facing to the pore interior, which can be selectively isomerize upon UV irradiation (Figure 1c). Consequently, the chiral pore interior of the network can undergo reversible deformation while maintaining the 2D frameworks in response to external stimuli, different from conventional chiral porous materials.[26–28]

Indeed, when circular dichroism (CD) spectroscopy experiments were subjected to the network structures, the solution of **1*S*** revealed a strong positive Cotton effect at longer wavelength range (Figure 2f), demonstrating that the slipped cofacial stacks of planar aromatic segments in a preferred direction and unidentical packing arrangements of the tetrapod aromatic segments at in-plane a and b axes

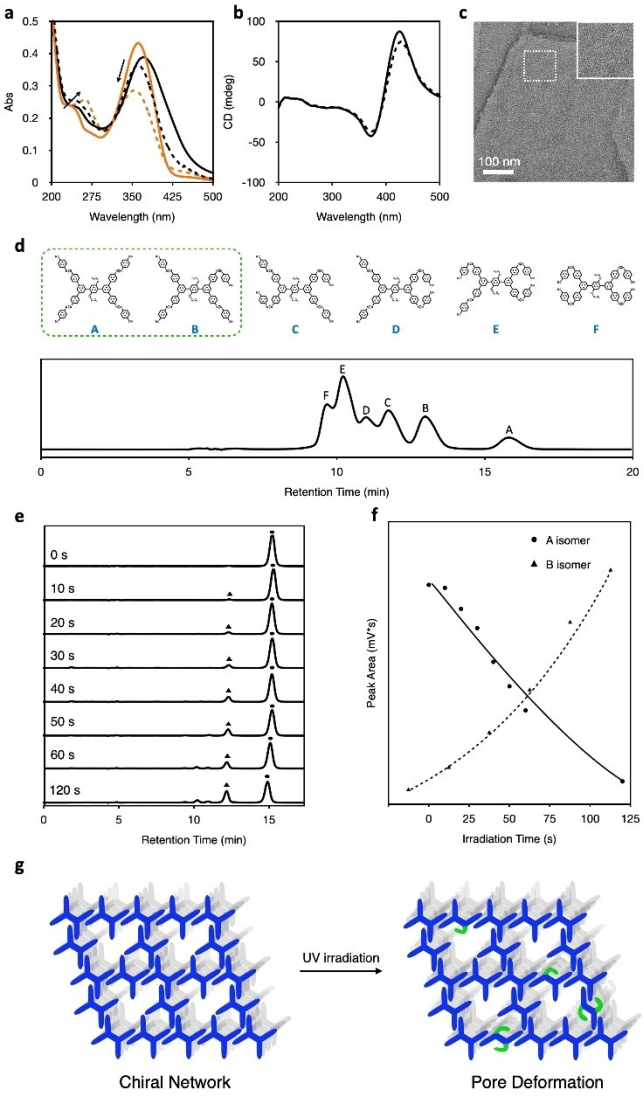

Figure 3. a) Absorption spectra of **1*S*** 0.01 wt%) in the dissolved state (in methanol solution; orange line) and assembled state (in aqueous methanol solution (3/7, v/v); black line) before (solid line) and after (dash line) UV irradiation. b) CD spectra of an aqueous methanol solution (3/7, v/v) of **1*S*** (0.01 wt%) before (solid) and after (dash) 50s UV irradiation. c) Negatively stained TEM images of **1*S*** after 50s UV irradiation. d) HPLC chromatogram of the dissolved solution of **1*S*** (0.01 wt% in methanol) with different molecular conformations after UV irradiation for 1 min. e) Time-dependent HPLC chromatograms of the assembled state of **1*S*** (0.01 wt% in aqueous methanol solution (3/7, v/v)) as a function of UV irradiation time (●: A isomer; ▲: B isomer). f) Conversion and formation of A and B isomers with UV irradiation. g) Schematic representation of the deformation of chiral pores by UV irradiation.

generate a chiral 2D superstructure. The sheet solution of **1*R*** formed from the enantiomer shows an opposite CD signal with a perfect mirror image relationship, indicating that the chirality information of the dendrimer chain transfers to the aromatic packings to form chiral 2D network structures.

Combined together, we propose that the slipped cofacial stacks of the coplanar aromatic segments lead to aromatic

clusters with hydrophobic side faces which laterally assemble with AA packing in *a*-axis and AB packing in *b*-axis (Figure 2e). Consequently, the parallel arrangement of the clusters relative to a layer plane generates network structure with four sublayers with slipping. Due to the slipping in a preferred direction of the sublayers, the unidentical packings in a and b directions induces chirality of a 2D network structure with a lack of both symmetry plane and inversion symmetry (Figure 2g). The spontaneous inversion symmetry breaking in 2D layer structures is very rare and has been reported in only a few systems, such as twisted graphene bilayers and hetero-bilayers of graphene with boron nitride layer.[29,30]

Considering the pore shape with protruded azobenzene side parts, we envisioned that UV irradiation can isomerize selectively the azobenzene units in the protruded parts while maintaining trans geometry at the 2D framework because of more exposed protruded parts to external environment than those of the interconnected framework (Figure 3g). Accordingly, we investigated the isomerization behavior of the *trans*-azobenzene units in the network by UV irradiation as a function of time. Upon irradiation of the dissolved state of **1** with UV light ($\lambda = 365$ nm), *trans*-to-*cis* isomerization undergoes as confirmed by a decrease of the π-π* absorption band at $\lambda_{max} = 370$ nm, accompanied by an increase in the absorbance in the higher energy region at around 270 nm.[31] The absorption behavior upon UV irradiation in the self-assembled state shows apparently smaller change compared with that of the dissolved state (Figure 3a). Remarkably, CD shows the signal to retain without apparent reduction upon UV irradiation (Figures 3b,S5). In addition, TEM and SAXS investigations show that the network structure with a pore lattice maintains without compromising its original 2D structure even after 50s UV irradiation (Figures 3c,S5,S6). These results suggests that the isomerization of the azobenzene units occurs selectively in the protruded parts of the interior within a certain time, while maintaining *trans*-form in the 2D frameworks. To gain insight into the isomerization of the azobenzene units in the network structure, we carried out HPLC experiments with the network solutions of **1** as a function of UV irradiation time. Indeed, HPLC shows that UV irradiation for 50s of the solution generates a predominant peak associated with mono-isomerization at the expense of the *trans*-isomer (Figure 3e,f), implying that the isomerization undergoes selectively at the azobenzene units of the protruded part in the pore while maintaining 2D network structure. When irradiation time was increased to 1 min, trace amounts of di-isomerization peaks can be detected from network solution (Figure 3e). In sharp contrast, the dissolved solution of **1** shows multiple isomerization peaks in HPLC under the identical irradiation condition (Figure 3d).[31] These results suggest that aromatic amphiphile **1** self-assembles into a single-layered network with photo switchable internal pores through selective isomerization of the azobenzene units of the protruded parts without compromising the network structure (Figure 3g), distinct from photoactive 3D materials based on multiple azobenzene units.[32,33]

HPLC investigations showed that, when irradiated UV light for 50s, approximately 25 % of *trans*-isomers participate in isomerization into *cis*-isomers (Figure 3e), suggesting that about one protruded azobenzene parts per pore in each sublayer can be considered to undergo *cis*-isomerization in this experimental condition. This result together with TEM and SAXS investigations indicates that the UV-irradiation within 1 min results in the deformation of chiral pore structure while retaining 2D frameworks. Upon short-wavelength UV irradiation (254 nm), the *cis*-isomer can recover to *trans*-isomers (Figure S7), indicative of reversible pore deformation.

We considered that the reversible deformation of the chiral interior would function as enantioselective capture and release. To investigate the capability of porous networks for enantioselective encapsulation, we selected hydrophobically substituted phenyl alanine (Fmoc-phenylalanine, Fmoc-Phe) because the pores consist of a hydrophobic aromatic interior.[21] The encapsulation of the guest in the chiral pore was monitored by tracing HPLC after the untrapped guest was removed by Sephadex column separation. We found that the 2D network shows about 97 % uptake of Fmoc-Phe with *L*-form (Figure S8), indicating that the uptake capacity is nearly perfect. This result explains that the single layer network structure consists of homochiral pores, consistent with the proposed structure based on X-ray and TEM investigations. The uptake capacity was further confirmed by titration experiments using an enantiopure phenylalanine guest that showed near-perfect uptake (Figure S9).

When the racemic solution was subjected to chiral HPLC, the porous networks of **1*S*** exclusively uptake the *L*-form with perfect inclusion preference over the *D*-form, while the networks based on **1*R*** capture only an opposite enantiomer (Figure 4a), indicative of excellent enantioselectivity for Fmoc-Phe. In contrast, both uptake capacity and enantioselectivity of the larger guest, Fmoc-protected tryptophan (Fmoc-Trp) showed to be lower than those of Fmoc-Phe (Figure S10). In the case of a smaller guest, Fmoc-alanine, the network structure does not exhibit any apparent inclusion activity, indicating that the network shows, not only enantioselectivity, but also size selectivity.

To substantiate the switching behavior of the pores driven by UV irradiation, release experiments were performed with **1*S*** network encapsulating *L*-enantiomer of Fmoc-Phe. After UV irradiation for 50s and then collecting the sheet fractions using a Sephadex column, HPLC measurements show the signals corresponding to the 2D network structures with traceless guest molecules (Figure 4b), demonstrating that the entrapped guest is released out of the pore interior. The release of the guest upon UV irradiation was further confirmed using 1D-Nuclear Overhauser effect (NOE) (Figure 4c). Consistent with the HPLC results, 1D-NOE spectra show a prominent peak at 7.31 ppm associated with the strong correlation between Ha of the host and H1 of the phenyl group in the *L*-guest, which disappears upon UV irradiation for 50s. This result indicates that the 2D network materials can absorb only one

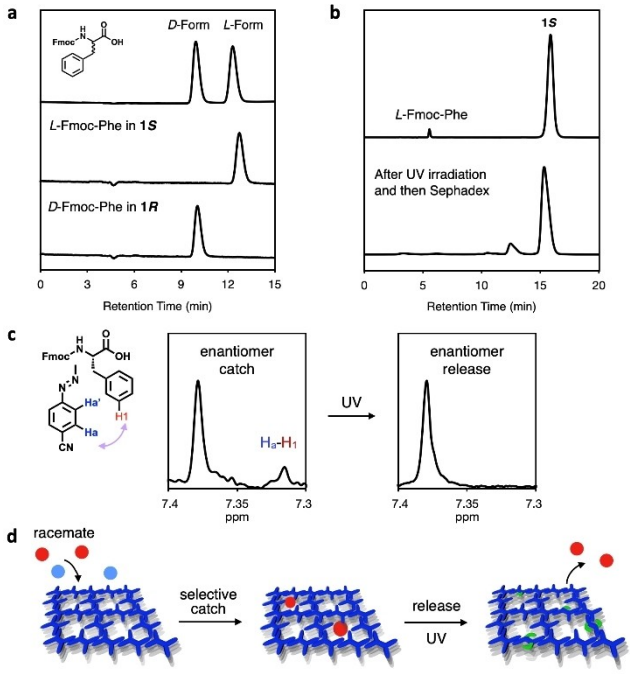

Figure 4. a) Chiral-HPLC traces of a racemic Fmoc-Phe (up), selective uptake of the *L*-form by **1*S*** (middle), and selective uptake of the *D*-form by **1*R*** (down) in aqueous methanol solution (3/7, v/v). b) HPLC spectra for the uptake and release of the *L*-form by **1*S***. c) Partial 1D NOE NMR spectra for the uptake (left) and release (right) of the *L*-form by **1*S*** in methanol-d_4/THF-d_8 (9/1, v/v). d) Schematic representation of the enantioselective encapsulation from a racemate and then release triggered by UV irradiation.

enantiomer in a racemic solution and then release by irradiating UV light (Figure 4d).

Conclusion

In conclusion, we have constructed single layer chiral network structures with switchable homochiral pores by the self-assembly of an azobenzene-based tetrapod aromatic amphiphile. The 2D networks consist of quadruple sublayers based on slipped packing in a preferred direction in which the sublayer has AA packing in *a*-axis and AB packing in *b*-axis to break both the plane and inversion symmetry, thereby resulting in chirality induction in the 2D network assembly. Moreover, this packing arrangement allows for protruded azobenzene segments in pores to participate in selective photo-isomerization, giving rise to reversible deformation of the chiral pore. Thus, the 2D network is capable of performing enantioselective capture and release triggered by light. We believe that our discovery paves the way for the construction of 2D chiral networks with complex pore functions capable of selective encapsulation, delivery, and then release.

Acknowledgements

This work was supported by the National Natural Science Foundation of China (22150710515, 92156023, 21971084 and 22171052), The Science and Technology Commission of Shanghai Municipality (22520712300), Fudan Research Fund and Project funded by China Postdoctoral Science Foundation (2020TQ0067 and 2020M681145).

Conflict of Interest

The authors declare no conflict of interest.

Data Availability Statement

The data that support the findings of this study are available from the corresponding author upon reasonable request.

Keywords: Chirality Induction · Enantioseparation · Self-Assembly · Supramolecular Networks · Switchable Pores

[1] J.-S. M. Lee, A. I. Cooper, *Chem. Rev.* **2020**, *120*, 2171–2214.
[2] Y. Gu, J. Zhao, J. A. Johnson, *Angew. Chem. Int. Ed.* **2020**, *59*, 5022–5049; *Angew. Chem.* **2020**, *132*, 5054–5085.
[3] A. M. Evans, M. J. Strauss, A. R. Corcos, Z. Hirani, W. Ji, L. S. Hamachi, X. Aguilar-Enriquez, A. D. Chavez, B. J. Smith, W. R. Dichtel, *Chem. Rev.* **2022**, *122*, 442–564.
[4] J.-H. Dou, M. Q. Arguilla, Y. Luo, J. Li, W. Zhang, L. Sun, J. L. Mancuso, L. Yang, T. Chen, L. R. Parent, G. Skorupskii, N. J. Libretto, C. Sun, M. C. Yang, P. V. Dip, E. J. Brignole, J. T. Miller, J. Kong, C. H. Hendon, J. Sun, M. Dincă, *Nat. Mater.* **2021**, *20*, 222–228.
[5] K. Baek, G. Yun, Y. Kim, D. Kim, R. Hota, I. Heang, D. Xu, Y. H. Ko, J. H. Suh, C. G. Park, B. J. Sung, K. Kim, *J. Am. Chem. Soc.* **2013**, *135*, 6523–6528.
[6] Z. Zhang, Y. Ye, S. Xiang, B. Chen, *Acc. Chem. Res.* **2022**, *55*, 3752–3766.
[7] B. Wang, R.-B. Lin, Z. Zhang, S. Xiang, B. Chen, *J. Am. Chem. Soc.* **2020**, *142*, 14399–14416.
[8] X. Liu, X. Zhou, B. Shen, Y. Kim, H. Wang, W. Pan, J. Kim, M. Lee, *J. Am. Chem. Soc.* **2020**, *142*, 1904–1910.
[9] M. Pfeffermann, R. Dong, R. Graf, W. Zajaczkowski, T. Gorelik, W. Pisula, A. Narita, K. Müllen, X. Feng, *J. Am. Chem. Soc.* **2015**, *137*, 14525–14532.
[10] J. Dong, L. Liu, C. Tan, Q. Xu, J. Zhang, Z. Qiao, D. Chu, Y. Liu, Q. Zhang, J. Jiang, Y. Han, A. P. Davis, Y. Cui, *Nature* **2022**, *602*, 606–611.
[11] S. Wang, Q. Wang, P. Shao, Y. Han, X. Gao, L. Ma, S. Yuan, X. Ma, J. Zhou, X. Feng, B. Wang, *J. Am. Chem. Soc.* **2017**, *139*, 4258–4261.
[12] K.-D. Zhang, J. Tian, D. Hanifi, Y. Zhang, A. C.-H. Sue, T.-Y. Zhou, L. Zhang, X. Zhao, Y. Liu, Z.-T. Li, *J. Am. Chem. Soc.* **2013**, *135*, 17913.
[13] Y. Li, Y. Dong, X. Miao, Y. Ren, B. Zhang, P. Wang, Y. Yu, B. Li, L. Isaacs, L. Cao, *Angew. Chem. Int. Ed.* **2018**, *57*, 729–733; *Angew. Chem.* **2018**, *130*, 737–741.
[14] R. Dong, T. Zhang, X. Feng, *Chem. Rev.* **2018**, *118*, 6189–6235.
[15] X. Liu, H. Li, Y. Kim, M. Lee, *Chem. Commun.* **2018**, *54*, 3102–3105.

[16] R.-R. Liang, S.-Y. A R.-H. Jiang, X. Zhao, *Chem. Soc. Rev.* **2020**, *49*, 3920–3951.
[17] B. Shen, Y. Kim, M. Lee, *Adv. Mater.* **2020**, *32*, 1905669.
[18] X. Han, J. Zhang, J. Huang, X. Wu, D. Yuan, Y. Liu, Y. Cui, *Nat. Commun.* **2018**, *9*, 1294.
[19] C.-J. Kim, A. Sánchez-Castillo, Z. Ziegler, Y. Ogawa, C. Noguez, J. Par, *Nat. Nanotechnol.* **2016**, *11*, 520–524.
[20] E. Y. Andrei, A. H. MacDonald, *Nat. Mater.* **2020**, *19*, 1265–1275.
[21] B. Sun, Y. Kim, Y. Wang, H. Wang, J. Kim, X. Liu, M. Lee, *Nat. Mater.* **2018**, *17*, 599–604.
[22] B. Sun, B. Shen, A. Urushima, X. Liu, X. Feng, E. Yashima, M. Lee, *Angew. Chem. Int. Ed.* **2020**, *59*, 22690–22696; *Angew. Chem.* **2020**, *132*, 22879–22885.
[23] X. Chen, Y. He, Y. Kim, M. Lee, *J. Am. Chem. Soc.* **2016**, *138*, 5773–5776.
[24] X. Feng, B. Shen, B. Sun, J. Kim, X. Liu, M. Lee, *Angew. Chem. Int. Ed.* **2020**, *59*, 11355–11359; *Angew. Chem.* **2020**, *132*, 11451–11455.
[25] M. Miyata, N. Tohnai, I. Hisaki, *Molecules* **2007**, *12*, 1973–2000.
[26] J. L. Segura, S. Royuela, M. M. Ramos, *Chem. Soc. Rev.* **2019**, *48*, 3903–3945.
[27] X. Han, C. Yuan, B. Hou, L. Liu, H. Li, Y. Liu, Y. Cui, *Chem. Soc. Rev.* **2020**, *49*, 6248–6272.
[28] H. Chen, Z.-Z. Gu, J. Zhang, *J. Am. Chem. Soc.* **2022**, *144*, 7245–7252.
[29] M. Yankowitz, Q. Ma, P. Jarillo-Herrero, B. J. van der W. LeRoy, *Nat. Rev. Phys.* **2019**, *1*, 112–125.
[30] L. Du, T. Hasan, A. Castellanoos-Gomez, G.-B. Liu, Y. Yao, C. N. Lau, Z. Sun, *Nat. Rev. Phys.* **2021**, *3*, 193–206.
[31] A. Galanti, J. Santoro, R. Mannancherry, Q. Duez, V. Diez-Cabanes, M. Valášek, J. De Winter, J. Cornil, P. Gerbaux, M. Mayor, P. Samori, *J. Am. Chem. Soc.* **2019**, *141*, 9273–9283.
[32] A. H. Heindl, J. Becker, H. A. Wegner, *Chem. Sci.* **2019**, *10*, 7418–7425.
[33] M. Baroncini, S. d'Agostino, G. Bergamini, P. Ceroni, A. Comotti, P. Sozzani, I. Bassanetti, F. Grepioni, T. M. Hernandez, S. Silvi, M. Venturi, A. Credi, *Nat. Chem.* **2015**, *7*, 634–640.
[34] A. B. Kanj, J. Bürck, S. Grosjean, S. Bräse, L. Heinke, *Chem. Commun.* **2019**, *55*, 8776–8779.

Manuscript received: January 13, 2023
Accepted manuscript online: March 7, 2023
Version of record online: March 27, 2023